Overview of the platform for experimentation and awareness-raising on fire risks at wildland urban interfaces (EXPLORII platform)

V. Tihay-Felicelli[a], T. Barboni [a], F. Morandini [a], P.A. Santoni [a], A. Pieri [a], C. Luciani [a], B. Martinent [a], A. Graziani [a], Y. Perez-Ramirez [a], N. Chiaramonti [a], M. Setti [b]

[a] University of Corsica, CNRS UMR 6134 SPE, Campus Grimaldi, BP 52, 20250 Corte, France

[b] Service d'Incendie et de Secours de la Haute-Corse (SIS2B), Casetta, 20600 Furiani, France

Corresponding author: V. Tihay-Felicelli, tihay_v@univ-corse.fr

Highlights

- The platform EXPLORII studies the vulnerability of buildings during a fire at WUI
- The platform can test building materials exposed to vegetation fire at full scale
- The platform is equipped with sensors to measure fire behaviour and fire impact
- The platform is equipped with analysers to quantify the smoke during a fire at WUI
- Heat fluxes and temperature are measured during the combustion of Douglas fir trees

Abstract

The aim of this article is to present a new experimental platform built by the University of Corsica in order to study the vulnerability of buildings to fires occurring at wildland urban interfaces. The platform is made up of a slope 10 m long by 6 m wide with an inclination of 20° and a flat surface located at its top hosting an instrumented single-storey house. The platform is equipped with different kinds of sensors: meteorological station, anemometers, load cell, heat flux gauges, thermocouples, cameras and smoke chemicals analysers. They allow obtaining experimental data on the burning of fuels and on the impact of fire on the buildings. Having a full-scale platform for studying fires at the wildland-urban interface (WUI) is important, particularly in terms of minimizing damage. By recreating realistic conditions and complex interactions between wildland fires, ornamental vegetation and residential areas, researchers can analyse and understand the mechanisms of fire spread in these vulnerable environments. In addition, a platform such as this enables testing and assessment of prevention and protection measures, such as fire-resistant building materials. Two experiments have been carried out to commission the platform with Douglas fir trees and test the experimental device. They have highlighted the protective effect of shutters, but also the role of double glazing as a thermal screen. The analysis of these first results has enabled improvements to be proposed to the experimental facility in order to better quantify the aerology and the heat fluxes impacting the building.

Keywords: platform, WUI, vulnerability of construction, fire, safety distance, smoke analysis

1 Introduction

Wildfires occur at the intersection of dry weather, available fuel and ignition sources [1,2]. Due to climate change that extends the dry and hot seasons [3] and the increasing pressure of human activities on the forest which result in increased sources of ignition [1,4], the severity and frequency of large fires has increased dramatically worldwide. Some of them have impacted the built environment sometimes resulting in fatalities [4–6]. In order to understand why human and material losses occur during fires at Wildland Urban Interfaces (WUI), post-fire studies have been carried out worldwide [7–14]. These works have attempted to reconstruct the timeline of the wildfire, to list the defensive actions and to carry out a survey of both victims and destroyed or damaged buildings. The mode of attack of the fire (direct contact, radiation or firebrands) is also investigated. The surveys performed after large scale fire events, which resulted in significant building damage and/or losses, showed that the vulnerability of buildings depends on the materials used for the construction, those located in the surroundings (wood, plastic, furniture, etc.) and the building characteristics (openings, vents, etc.) [9]. Previous studies have also highlighted the critical role of the ornamental vegetation (trees, shrubs or hedges) [13] and fences [7] during the spread of the fire from wild environment towards the buildings. In addition, the important role of topography and weather conditions on the damage or destruction of buildings has also been underlined [9]. Regarding the victims, the investigations reported by Vacca et al. [4] revealed that most of those injured suffered from burns and smoke intoxication. During a wildfire, smoke contains gases, particles, and volatile organic compounds (VOCs) that can be toxic and dangerous to health [15–18]. To prevent the risk of fire at the wildland-urban interface, there are recommendations (or laws) for residents to limit the spread of fire toward buildings (positioning plants in the home ignition zone [19–23]) or to limit the entry of smoke in the event of a fire (closing doors, placing towels under doors, etc.). In some countries, building codes and standards already include requirements intended to reduce the ignition risk of structures [24–27]. However, the devastating effect of current large outdoor fire events is revealing weaknesses in existing building codes and standard testing methodologies on the basis of which building codes are developed [28]. To reduce the impact of wildfires on people and buildings, it is therefore necessary to (i) make structures more resistant to fire, taking into account the typical pathways of a fire (radiant exposure, direct flame contact and firebrand attack [29]), (ii) better define the landscaping around the buildings and (iii) adopt measures to limit the penetration of smoke into buildings.

To our knowledge, there have been few experimental studies on the impact of outdoor fires on structures. The elements studied are mainly wooden walls [30–32], roofs [33,34], vents [35], decking assemblies [36–39] or windows [40–44]. As for other types of hazards such as floods, winds or earthquakes [45–47], platforms have emerged across the world in recent years to assess and mitigate fire attacks on structures. There are large-scale experimental fire facilities at the National Fire Research Laboratory in USA (NIST) [48], the Building Research Institute (BRI) in Japan (National Research and Development Agency) [49], the National Research Institute of Fire and Disaster (NRIFD) in Japan [50] or the National Bushfire Behaviour Research Laboratory at CSIRO in Australia [51]. The National Fire Research Laboratory (NFRL), developed by NIST, is a 3800 m^2 building with an Emissions Control System (ECS) to handle smoke and combustion products [52]. The NFRL is capable of conducting experiments with very tall elements (such as buildings up to two full stories). It has four large fire calorimeters to measure the heat release rate of fires from 20 kW to 20,000 kW. Measurements of temperature, heat flux, strain, force and displacement are made to characterise the behaviour of structures in fire. The BRI has two main experimental facilities for large-scale fire experiments. The first is a fire wind tunnel (FRWTF) with a 4 metre diameter fan that can

reach wind speeds of up to 10 m/s. This facility allows the influence of wind on the fire behaviour of buildings and the ignition of firebrands to be studied [53]. The NIST Firebrand Generator (NIST Dragon) for example, was characterised at this location [54]. The second facility consists of a fire hall with a floor area of 720 m² and a ceiling height of 27 m [55]. Fire tests are carried out to understand how fire spreads from the fire source to the whole room and to assess the fire resistance of structures. The results obtained are used in the definition of Japanese technical standards and/or the formulation of government policy for buildings. The NRIFD has several experimental facilities dedicated to fire research [50]. There are two buildings for the large experiments. The large fire test building, with an experimental area of 24 m × 23 m × 20 m, allows fire and combustion experiments to be conducted indoors. The fire extinguishing research building has a primary experimental area of 25 m × 25 m × 22 m and a secondary experimental area of 14 m × 14 m × 12 m. With its large blower, experiments can be carried out on the spread of fire under windy conditions. The National Bushfire Behaviour Research Laboratory at Black Mountain, Canberra is home to the CSIRO Pyrotron. The Pyrotron is a 25-metre-long-combustion wind tunnel with a working section of 2 m × 4.8 m × 2 m. It can achieve air speeds up to 5.3 m/**s** and was designed to enable the safe and repeatable investigation of the mechanisms of flame propagation in bushfire fuels [56]. The CSIRO in collaboration with Suncorp, James Cook University (the Cyclone Testing Station and Centre for Disaster Studies) and Room 11 Architects is also involved in the One house project [57]. The materials of this house are designed to be resilient to water, wind and fire. This involves using steel framing, cladding and roof sheeting, durable insulation, aerated concrete panels and a concrete slab. Burners are used to create a 12-metre wide fire front. More than 50 heat sensors measure air and surface temperatures. Taking into account the existing experimental facilities described above, there seems to be a lack of outdoor platforms for testing the vulnerability of buildings to fire at the Wildland Urban Interfaces (WUI) under conditions close to reality, i.e. with vegetation or secondary fuels (such as garden sheds, fences, terraces, etc.). This is why the University of Corsica has built an outdoor platform for experimentation and awareness-raising in fire risks at a WUI called the platform EXPLORII (Plateforme d'EXpérimentations, de sensibiLisation et de fOrmation aux Risques Incendie dans les Interfaces). The aim of this platform is to study the impact of a fire on dwellings located at a Wildland Urban Interface by (i) Obtaining experimental data on the burning of fuels (plants and secondary structures) located near buildings, (ii) Collecting experimental data on the vulnerability of the constructive elements of a building facing fires from burning plants or secondary structures to define safety distance, (iii) Studying the composition of smoke inside and outside a house in the vicinity of a fire, (iv) Collecting experimental data for the calibration of detailed models of fire propagation and (v) Raising awareness among fire prevention stakeholders and the general public. The platform has therefore been developed to be flexible in order to test several types of materials (terrace, cladding, joinery, gutters, etc.) and fuels (hedges, trees, fence, secondary structure, etc.).

The aim of this article is to present the EXPLORII platform and the two experiments carried out for its commissioning with Douglas fir trees. The results of these tests will show the potential of the experimental device to study the impact of a vegetation fire on a building, taking into account the wind characteristics. To this end, measurements will be made of the direction and speed of the wind, the mass loss of the Douglas firs during their burning, the total and radiant fluxes received by the building, and the temperatures of the openings. These initial measurements will also make it possible to highlight the limitations of the experimental device and propose improvements, as well as provide some data on the effect of shutters and double glazing on the impact of a fire on the joinery. The experimental design is first described and then the results obtained during the test phase are presented and discussed.

2 Methodology

2.1 Experimental design

The platform was built in Corte (GPS coordinates: 42°18'11.3"N 9°10'13.8"E) on land made available to the University of Corsica by the Service d'Incendie et de Secours de la Haute-Corse (Fire and Rescue Service of Corsica). It was commissioned in May 2022. The experimental design of the platform aims to enable the study of the impact of a fire from ornamental vegetation, fences or secondary structures on a building and its constituent elements. For this, the construction has a modular design to allow the study of different construction elements such as windows, shutters, cladding, gutters, roof coverings, terraces, etc. The dimension of the platform is 20 m × 25 m. This space is made up of a slope 10 m long by 6 m wide with an inclination of 20° and a flat surface located at the top (Figure 1). The plateau hosts an instrumented single-storey house built of concrete 7 m long by 3.8 m wide and a terrace 7 m long by 3 m wide. The building has a controlled mechanical ventilation system. The facade facing the slope has three openings measuring 0.6 m × 0.95 m. These openings can accommodate different types of material: PVC, aluminium, wood with or without shutters. There is also a 20-foot container on the platform to store the fuel used for the experiments. The interior of the house is divided into three parts: a control area of 4.7 m², a storage area of 4.1 m² and an instrumentation area of 15.9 m² at the level of the openings. The control area is dedicated to the real-time monitoring of the data collected during the experiments and is separated from the instrumentation area by a window. An elaborate set of sensors has been designed to measure the atmospheric conditions near the fire (air temperature, relative humidity, wind speed and wind direction), the fire behaviour (fuel mass loss, fire front geometry and rate of spread), the effect of the fire on the building (radiant and total heat fluxes, surface temperature) as well as the smoke emitted during the experiments (gases and particles). A detailed description of the different sensors is included in Table 1.

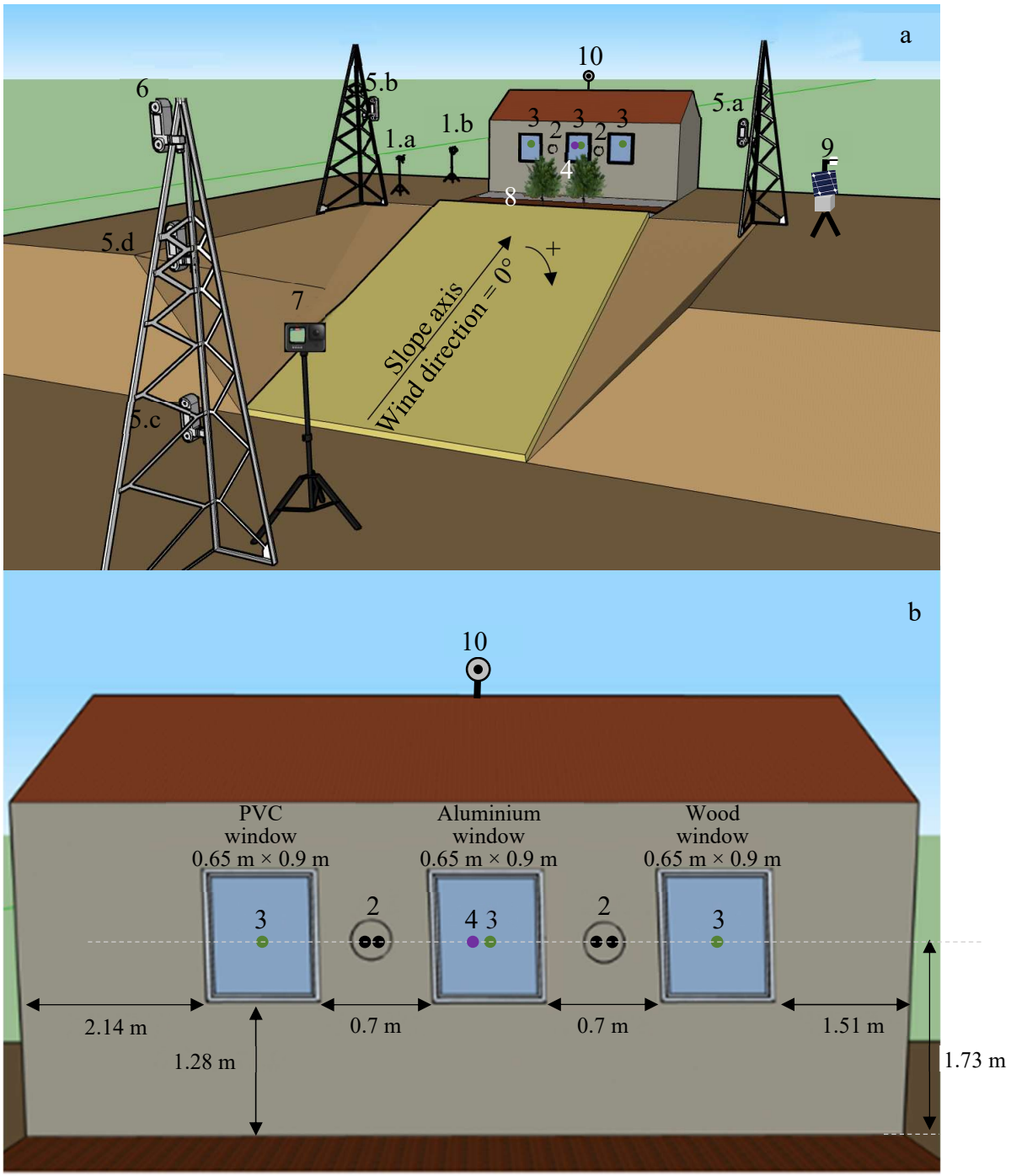

Figure 1: Diagram of the experimental device of the EXPLOII platform a) General view b) View of the exposed facade - 1: Cameras. 2: Pairs of total and radiant heat flux gauges. 3: K-type surface thermocouple 4: Radiant heat flux gauge. 5: 2D sonic anemometer. 6: 3D anemometer. 7: Go Pro. 8: Load Cell. 9: Weather station. 10: Sampling rod for the outdoor smoke analysers

Table 1: Description of the sensors used on the EXPLORII platform (u_x, u_y, u_z are the velocity components along x, y, z directions respectively, u is the wind speed and θ the wind angle with respect to the axis of the slope)

Sensors	Sensor type, manufacturer and model	Variables and measurement range	Measurement height range (m above the ground level)	Sampling frequency (Hz)	Accuracy
Main mast (10 m)	3D sonic anemometer (CSAT3B, Campbell Scientific, Inc.)	u_x, u_y, u_z (up to 65.535 m/s)	10	1	Direction: ±0.7° Speed:< ±4cm/s for u,v and 8cm/s for w
	2D sonic anemometer (WindSonic1 Gill, Campbell Scientific, Inc.)	u (0 to 60 m/s), θ (0 to 360°)	2 and 6	1	Direction: ±3° Speed: ±2%
Short masts (7m)	2D sonic anemometer (WindSonic1 Gill, Campbell Scientific, Inc.)	u (0 to 60 m/s), θ (0 to 360°)	2	1	Direction: ±3° Speed: ±2%
Nomadic tower	Air temperature and relative humidity sensor (EE181 Campbell Scientific)	Temperature (-40°C to +60°C) and relative humidity (0 to 100%)	1	1	Temperature: ±0.2°C Humidity: ± 1.3%
	Fuel moisture sensor with a 10hr stick (CS506 Campbell Scientific, Inc.)	Fuel moisture content (0 to 70%)	1	1	Range 0-10%: ± 1.25% Range 10-20%: ± 2% Range 20-30%: ± 3.4% Range 30-50%: ± 4.11%
	Pyranometer (SR 05 Campbell Scientific, Inc.)	Solar radiation (0 to 1600 W/m²)	1	1	<1.8 %
Fire behavior characterization	Load cell (SQB load cells (EXA))	Mass (up to 150 kg)	0	1	20 g
Flame geometry observation	Camera Hero 10 Black (Gopro)	Fire front shape and velocity	10	1	
	Camera EOS 6 (Canon) equipped with a Canon RF 24-105 mm f/4 lens	Flame front geometry	1	1	
Fire impact	Total heat flux gauge 64-20-18 (MEDTHERM)	Heat flux on the façade (up to 200 kW/m²)	1.73	1	Time constant: less than 250 ms Heat flux: ± 3%

	Radiant heat flux gauge 64P-10-22 (MEDTHERM)	Heat flux on the façade (up to 100 kW/m²)	1.73	1	Time constant: less than 250 ms Heat flux: ± 3%
	Radiant heat flux gauge 64P-5-22 (MEDTHERM)	Heat flux inside the house (up to 50 kW/m²)	1.73	1	Time constant: less than 250 ms Heat flux: ± 3%
	K-type surface thermocouples 4 × 8 mm – DS48 series	Temperature (up to 375°C)	1.73	1	± 1.5°C
Smoke analysis outdoor	ELPI+ (Electrostatic Low Pressure Impactor; Addair)	Particles analyses (Particle size between 0.006 µm and 10 µm)	4.7	1	Measurement frequency up to 10 Hz Accuracy: ± 5%
	FTIR (Fourier-Transform Infrared Spectroscopy AA-4000 model Addair)	Gas analyses (50 gases)	4.7	1	Gas acquisition: 1 Hz Accuracy: ± 1% BaF2 window
	Multiparametric QA station (Ethera)	Gas analyses (PM_1, $PM_{2.5}$ – PM_{10}, SO_2, CO, CO_2, NH_3, PID (COV), NO_x)	4.7	1	Accuracy: ± 5%
	Tenax TA Tubes (Supelco) with pump sampling (Gilair plus) for off-lines analyses with ATD-GC/MS and FID (Flame ionization detector; TVA Thermofischer)	VOC (Tenax tube analyses with VOCs >C_5) Total Hydrocarbon (FID) Range: 1 to 10 000 ppmc	4.7		Accuracy GC/MS: ± 5% Accuracy for THC: 2%
Smoke analysis indoor	Fidas 200 (Addair)	Particles analyses (Particle size between 0.18 µm and 18 µm Mass: 1 – 10 000 µg/m^3)	1	1	Repeatability and accuracy: ± 5%
	MX6 ibrid Multigas (Industrial Scientific)	Gas analyses	1	1	Accuracy: ± 5%

		(CO_2, CO, NO, NO_2, HCN, NH_3, O_2, H_2, SO_2)			
	Tenax TA Tubes (Supelco) with pump sampling (Gilair plus) for off-lines analyses with ATD-GC/MS and FID (Flame ionization detector; TVA Thermofischer)	VOC (Tenax tube analyses with VOCs >C_5) Total Hydrocarbon (FID) Range: 1 to 10 000 ppmc	1		Accuracy GC/MS: ± 5% Accuracy for THC: 2%

3

2.2 Atmospheric measurements

To measure the wind conditions on the platform, a set of sensors located on different towers is used (5.a to 5.d in Figure 1). A 10 m high aluminium tower (main mast) is located down-slope in the centreline of the platform. A CSAT3B 3D sonic anemometer (Campbell Scientific, Inc.) is mounted at a height of 10 m on the main mast. This tower also includes two 2D sonic anemometers (WindSonic1 Gill, Campbell Scientific, Inc.) positioned at 2 m and 6 m from the ground. This experimental device provides the wind profile as a function of height at the bottom of the slope. This data is essential for understanding and modelling the incoming wind. In addition, two 7 m high aluminium masts are installed at the top of the slope on either side of the burning area. Each 7 m mast includes a 2D sonic anemometer (WindSonic1 Gill, Campbell Scientific, Inc.) placed 2 m above the ground. These two anemometers show the effect of the arrival of the fire on the aerology around the building. All anemometers are sampled at a frequency of 1 Hz using a Campbell Scientific, Inc. CR9000 data logger. For all the anemometers, a wind direction of 0° corresponds to a wind along the axis of the slope (i.e., the most favourable for the spread of fire towards the house).

To measure the ambient conditions, a weather station was installed on a movable tripod (Figure 1). This station consists of a CR6 data logger (Campbell Scientific, Inc.) connected to an air temperature and relative humidity sensor (EE181 Campbell Scientific, Inc.), a fuel moisture sensor with a 10hr stick (CS506 Campbell Scientific, Inc.) and a second-class pyranometer (SR 05 Campbell Scientific, Inc.). The weather station is equipped with a solar panel to be autonomous and a 2G/3G connection to retrieve data remotely.

2.3 Measurements of the fire behaviour and fire impact

To record the spread of the fire front during the experiments, a GoPro camera (Hero 10 Black) is installed at the bottom of the slope on a telescopic mast with a height of up to 15 m (Figure 1) which is equipped with a motorised head to adjust the vertical tilt and the horizontal panning of the camera. The GoPro camera allows observing the rear of the fire front spreading upslope towards the hedge. The sampling frequency of the GoPro camera is set to 1 Hz in order to record one image every second. Two cameras (Canon EOS 6) equipped with a Canon RF 24-105 mm f/4 lens are also placed at the top of the slope on the side in order to observe the combustion at the level of the load cell. The first camera (1.a in Figure 1) allows the characterization of the geometry of the flame front when the vegetation, the fence or the secondary structure burns. The second camera (1.b in Figure 1) makes it possible to visualize the spread of the fire in the vegetation, the fence or the secondary structure during the test. These cameras take an image is every second. To simplify image processing, the three devices (GoPro camera and the 2 cameras) are synchronised.

To assess the number and size of firebrands impacting the surroundings of the house, stainless steel trays measuring 2 m × 0.5 m × 0.1 m are placed in the centre of the terrace, at the side and at the rear of the house, 1 m from the facade. The trays are filled with water to ensure that the firebrands are extinguished as soon as they come into contact with the trays. The firebrands are then dried in an oven at 110°C for 24 hours, after which the size of the firebrands is measured using callipers and the dry mass is determined using a precision balance.

The mass loss of the burning fuels is measured using a load cell 7 m long and 1 m wide. It is placed adjacent to the top of the slope at a distance of 3 m from the facade (Figure 1). The load cell is made up of 2 stainless steel plates. Each one is equipped with 2 SQB load cells (EXA),

which are connected to an ENOD4 digital transmitter (Scaime) with a 4/20 mA analogue output. The load cell assembly is covered with calcium silicate to protect it from heat. The total capacity of the load cell is 150 kg. Before each series of tests, the load cell is calibrated to the appropriate mass range for the tests using class M1 calibration weights. The accuracy of the load cell is 20 g. A 3-second moving average is applied to the mass to smooth the data. The mass loss rate (MLR) is then calculated using a centred differential. Based on the mass loss recorded by the load cell, the heat release rate (HRR) of the fire is calculated using the following equation:

$$HRR = MLR \times \Delta H_{eff} \quad (1)$$

Where MLR is the mass loss rate calculated by the derivative of mass measurements as a function of time and ΔH_{eff} is the effective heat of combustion of the fuels. To calculate ΔH_{eff}, experiments are carried out in the laboratory using an LSHR apparatus. The fuel is placed on a load cell and ignited by a flame front propagating through a litter of wood wool. ΔH_{eff} is calculated with Eq. 1 from measurements of mass loss and HRR obtained by oxygen consumption calorimetry.

The impact of the fire on the construction and its elements is assessed with several measurement systems. Two pairs of MEDTHERM 64 Series heat flux gauges are mounted on the facade between the windows at a height of 1.73 m from the surface of the terrace (Figure 1). To this end, two holes were dug into the facade in order to pass the heat flux gauges through the wall (Figure 2). Each pair includes a total heat flux gauge (MEDTHERM model 64-20-18) with a measurement range of 0-200 kW/m² and a radiant heat flux gauge with a sapphire window (MEDTHERM model 64P-10-22) with a measurement range of 0-100 W/m². In order to determine the radiant heat flux transmitted across the windows, a radiant heat gauge with a sapphire window (MEDTHERM model 64P-5-22) is placed inside the building at the centre of the middle window (Figure 2). Its measuring range is 0-50 kW/m². All heat flux gauges are cooled with water at 20°C using a ThermoChill II LR recirculating chiller. To complete these devices, K-type surface thermocouples with Kapton cable (DS48 series) are positioned on the building openings (Figure 2). The sensitive element of the thermocouple is encapsulated in a high-temperature glue forming a 4 x 8 mm contact surface with a thickness of 2 mm. Its accuracy is ±1.5°C between -40 and 375°C. This model was chosen as it is inexpensive, reusable and highly flexible. In the case of windows or shutters, the thermocouples are placed at the centre on the interior and exterior sides. In order to avoid damaging the thermocouples located outside when the flame front reaches the house, a small piece of Kapton tape is taped over the surface thermocouples and the wires are covered with an aluminium foil. Finally, a K-type thermocouple is located at a height of 1.5 m in the centre of the house instrumentation area to assess a possible temperature increase inside the building.

The load cell, the heat flux gauges and the thermocouples are sampled at a frequency of 1 Hz using a Campbell Scientific, Inc. CR1000 data logger.

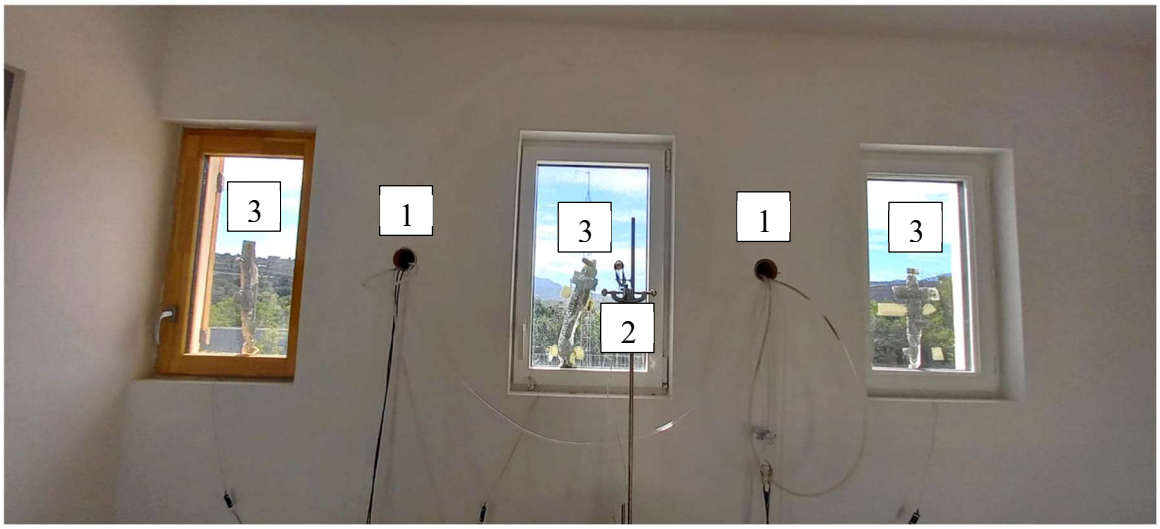

Figure 2: Photograph of the instruments taken from inside the building. 1: pair of total and radiant heat flux gauges. 2: radiant heat flux gauge. 3: K-type surface thermocouple.

2.4 Smoke analysis

Smoke from a fire at the WUI includes significant amounts of gases, aerosols (PM) and volatile organic compounds (VOCs). Accurately characterizing the source term is important for understanding the potential impacts of smoke on air quality and human health, as well as for designing effective control measures to mitigate these impacts. The diversity of compounds in the smoke induces the use of different equipment to characterize them. The setup dedicated to smoke analysis on the EXPLORII platform is composed of two sets. The first set of devices aims to characterize the source terms from smoke which refers to the amount and type of emissions released into the atmosphere from wildland fire. It includes an ELPI+ (Electrostatic Low Pressure Impactor; Addair) for the analysis of particles; a Fourier-Transform Infrared Spectroscopy AA-4000 model (Addair) and Multiparametric QA station (Ethera) for the gas analyses as well as Tenax TA Tubes (Supelco) with pump sampling (Gilair plus) coupled with off-lines analyses (ATD-GC/SM and FID) for VOC and Total Hydrocarbon analyses (Table 1). A sampling cane is placed on the roof of the house (Fig. 1) to sample the smoke during the fire spread. The smoke measuring devices are protected inside the house. The generation of combustion products is quantified in terms of emission factors, EF_i (g.kg^{-1}). Fire-integrated emission factors are calculated using the carbon and nitrogen mass balance approach. Thus, the emission factor of a species i is calculated from the ratio of the mass concentration of that species to the total carbon concentration or the total nitrogen concentration emitted in the smoke [58]:

$$EF_i = \frac{[C_i]}{\Sigma([C_{CO_2}]+[C_{CO}]+[C_{CH_4}]+[C_{NMOC}]+[C_a])} \times C_{fuel} \text{ for gases containing carbon} \quad (2)$$

Where C_{fuel} is the mass fraction of carbon in the fuel, C_i is the mass concentration of carbon constituent i emitted during the burning, C_{NMOC} corresponds to the non-methane organic compounds and C_a refers to the aerosols.

To evaluate the combustion completeness [59], the modified combustion efficiency (MCE) was introduced, as follows:

$$MCE = \frac{[CO_2]}{[CO_2]+[CO]} \quad (3)$$

where $[CO_2]$ and $[CO]$ are the molar concentrations of emitted CO_2 and CO in the smoke. Fire-integrated excess molar mixing ratios of CO_2 and CO are used to calculate mean modified combustion efficiencies.

The second set of devices is devoted to quantifying the smoke entering the house in order to assess the indoor air quality during and after the experiment. Fidas 200 (Addair), MX6 ibrid Multigas (Industrial Scientific) and Tenax TA Tubes (Supelco) with sampling by pump (Gilair plus) coupled with off-lines analyses (ATD-GC/SM and FID) are used to quantify respectively the aerosols (in numbers and particle size), gases and VOCs. Factors such as the size and number of openings, the use of a mechanical ventilation system, etc., can be studied by means of the platform EXPLORII. This can help for recommendations to home owners concerning the protective measures to reduce exposure to smoke, minimize health risks and improve indoor air quality after a fire.

2.5 Experimental procedure

Two commissioning experiments were carried out with Douglas fir trees to test the platform. The main objectives were to validate the performance of the sensors of the EXPLORII platform, to highlight the limitations of the experimental device and propose improvements. The experimental protocol was therefore designed to test the response of the load cell at different initial loads, to see the behaviour (resistance and non-detachment) of the thermocouples placed on the joineries of the building and to ensure that the number and the position of the sensors, in particular the heat flux gauges and the anemometers, were sufficient to monitor the impact of a vegetation fire on a building, and the characteristics of the wind before and during the burning tests. Figure 3 shows a diagram explaining the methodology used to achieve the above objectives with the two commissioning tests.

Table 2 shows the experimental setup used for the two commissioning tests.

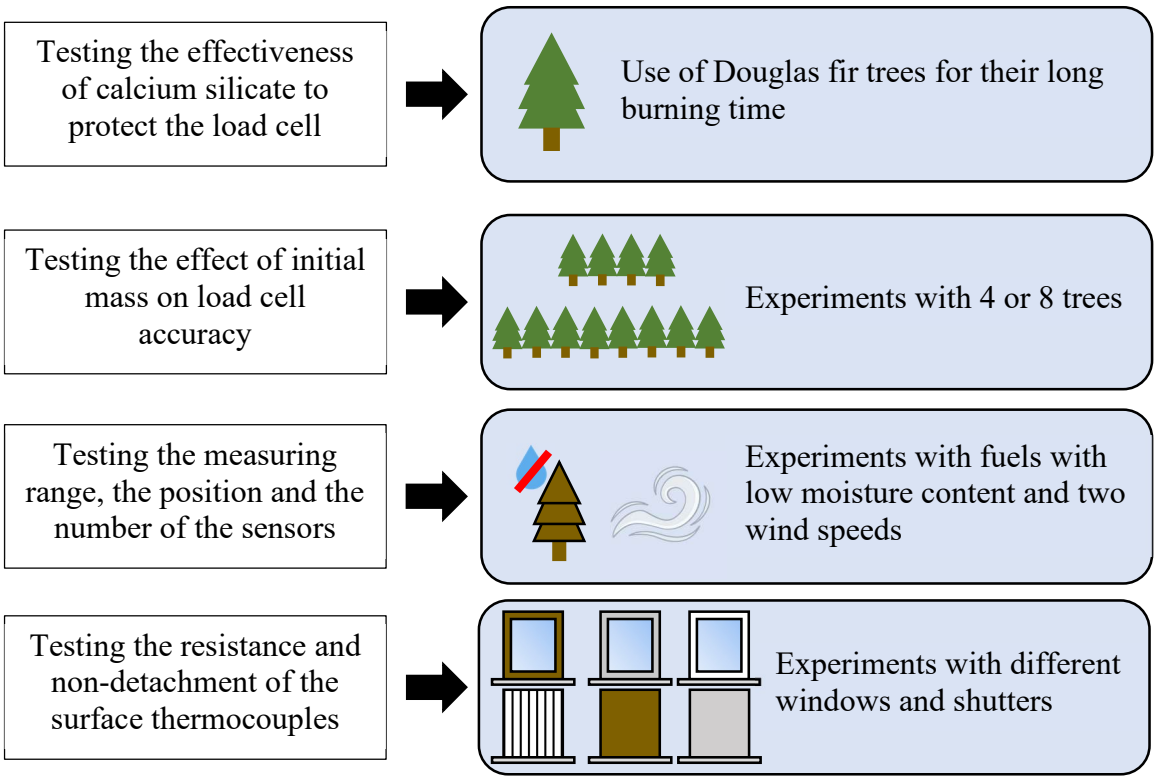

Figure 3: Diagram explaining the methodology of the commissioning tests

The Douglas fir trees were selected for their rather long combustion time compared to that of shrubs. This characteristic was interesting for testing the heat resistance of the calcium silicate plates protecting the load cell. We used 4 trees for test 1, corresponding to an initial mass of 17.4 kg, and 8 trees for test 2, corresponding to an initial mass of 68.9 kg. These two configurations were chosen in order to test two different initial masses within the measuring range of the load cell. The trees were placed 3 m from the facade next to each other in a welded mesh cage 2 m long by 1 m wide for test 1 and 6 m long by 1 m wide for test 2 (Figure 4). The trees were 1.4 (±0.19) m high. For both tests, to mimic the ignition of the trees due to a fire spreading across an herbaceous stratum, a litter of wood wool 5 m long was used with a fuel load of 1 kg/m². The litter was located in the slope. Its width corresponds to that of the trees: 2 m for test 1 and 6 m for test 2. The wood wool was ignited with a torch containing a gasoline/diesel mixture (1/3 gasoline - 2/3 diesel), which was applied over the entire length of the bed and a width of approximately 5 cm. 2.7 g and 13.6 g of the mixture were used to ignite the wood wool for tests 1 and 2, respectively. This amount allows efficient ignition without significantly affecting the spread of the front in the wood wool litter. The moisture content (MC) of the trees was 12.9 (±0.9) % (dry basis) and that of the wood wool was 5.7 (±0.4) % (dry basis). These low moisture contents allow significant heat release when the vegetation is burned. The ambient temperature was 15.8°C for test 1 and 22.0°C for test 2. The ambient relative humidity was 44.9 and 48.9% for tests 1 and 2 respectively. The mean wind speed calculated from the data of the anemometer 5.a over the whole duration of the tests was 2.6 (±1.0) m/s and 1.6 (±0.6) m/s for tests 1 and 2, respectively. The mean wind direction in relation to the axis of the slope calculated from the data of the anemometer 5.a over the whole duration of the tests was -4.8 (±38.4)° and -5.6 (±23.1)° for tests 1 and 2, respectively. As for the house, we did not install gutters on the building and the terrace was made of concrete. Double-glazed PVC, aluminium and wooden windows were installed on the facade exposed to the fire. Two configurations were tested for the opening: without shutters and with three aluminium shutters,

in order to verify that the surface thermocouples resisted and did not come off during the experiments.

Figure 4: Photograph of the Douglas fir trees a) Test 1 with 4 trees b) Test 2 with 8 trees

Table 2: Experimental configurations used to test EXPLORII platform

Test number	Number of trees	Initial mass (kg)	Ambient relative humidity (%)	Ambient temperature (°C)	Tree MC (%)	Wood wool MC (%)	Mean wind speed (m/s)	Mean wind direction (°)	Shutter configuration
1	4	17.4	44.9	15.8	13.8	6.1	2.6 (±1.0)	-4.8 (±38.4)	Aluminium
2	8	68.9	48.9	22.0	12.0	5.2	1.6 (±0.6)	-5.6 (±23.1)	Without shutter

The geometry of the flame front was determined by image processing with MATLAB® using camera 1.a situated on the side of the platform. The flame height (FH), the flame length (FL), the advance of the front of flame (FA) and the separation angle (β) were obtained using the following definitions (Figure 5):

- The flame length (FL) is the distance between the highest point of the flame envelope (point A) and the lowest point to the left of the flame (point B).
- The flame height (FH) is the distance between the lowest point on the left of the flame (point B) and point C, which is the projection of point A on the perpendicular to the ground crossing B.
- The advance of the flame front (FA) corresponds to the distance between the lowest point on the left of the flame (point B) and point D, which is the projection of point A on the ground.
- The separation angle (β) is the angle between the flame length (FL) direction and ground.

Since residual flames remain present during the extinction phase, it is difficult to determine the flame duration visually. We therefore preferred to define the flame duration as the time between the ignition of the trees and the moment when the mass loss rate (MLR) divided by the ground surface of the cage becomes lower than 20 g/s. The mean values calculated for the flame geometry correspond to the average during the flame duration.

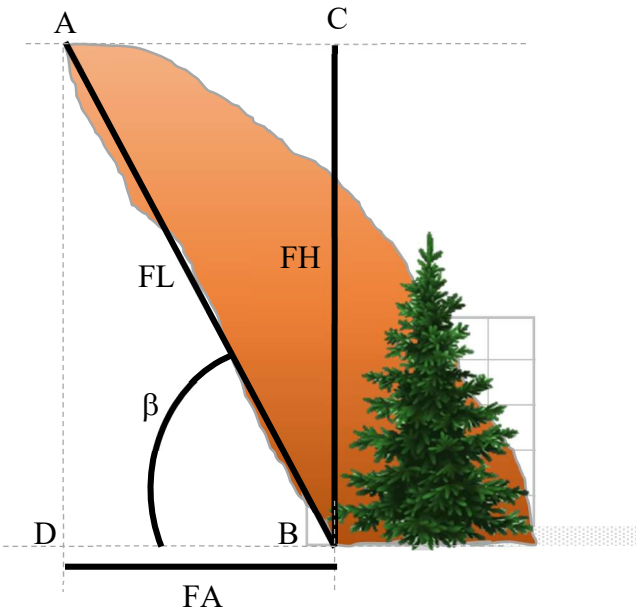

Figure 5: Geometry of the flame front

3 Experimental results

3.1 Observation of the fire behaviour and its interactions with atmosphere

The different stages of combustion observed during the experiments are shown in Figure 6 for both tests. The photographs were recorded by camera 1.a placed on the side of the platform. The time t=0 corresponds to the moment when the Douglas fir trees ignite. Table 3 shows the average values of the flame descriptors (FH, FL, FA and β) as well as the peak of the mass loss rate (PMLR), the time at which PMLR occurs (t_{PMLR}), the flame duration (t_f) and the final mass after the burning. The experiments begin with the propagation of the fire front across the wood wool, which is well captured by camera 1.c. The fire front has a V-shape due to the slope with a maximum flame height higher than 1 m (Figure 6Figure 7.a). The trees are ignited by direct contact with the flame front coming from the wood wool litter (Figure 6.b). The position of cameras 1.a and 1.b gives a good view of the Douglas fir ignition phase. The fire front then spreads within the trees very quickly (Figure 6.c). For test 1, a flame duration of 67 s is observed whereas 131 s is recorded for test 2. During the flaming stage, the flame length is on average equal to 1.4 m for test 1 and 2.1 m for test 2 with maximum values of 4.2 and 4.9 m, for test 1 and 2, respectively. The flames are therefore on average 1.5 times longer for test 2. The mean separation angle is 50.9 (±17.1)° for test 1 and 77.2 (±13.1)° for test 2. For test 2, the flames are therefore leaning less towards the building, in particular because of a lower wind speed. This also results in a lower advance of the flame front for case 2. For test 2, the flames do not reach the facade while they touch the roof in test 1 (Figure 6.c). The flame phase of Douglas fir combustion is well followed by camera 1.a. However, with larger loads or higher fuels, it will be necessary to move camera 1.a back to see the full height of the flame front. After the flameout, smoldering is observed (Figure 6.d). At the end of the experiments, only the trunks remain (Figure 7).

Table 3: Fire descriptors measured during the experiments with Douglas fir trees

Test number	PMLR (kg/s)	t_{PMLR} (s)	t_f (s)	Final mass (kg)	FH_{max} (m)	FH_{mean} (m)	FL_{max} (m)	FL_{mean} (m)	FA_{max} (m)	FA_{mean} (m)	β_{mean} (°)
1	0.59	9	67	6.47	3.2	1.1	4.2	1.4	3.1	0.9	50.9 (±17.1)
2	1.22	20	192	15.1	4.5	2.1	4.9	2.1	2.4	0.5	77.2 (±13.1)

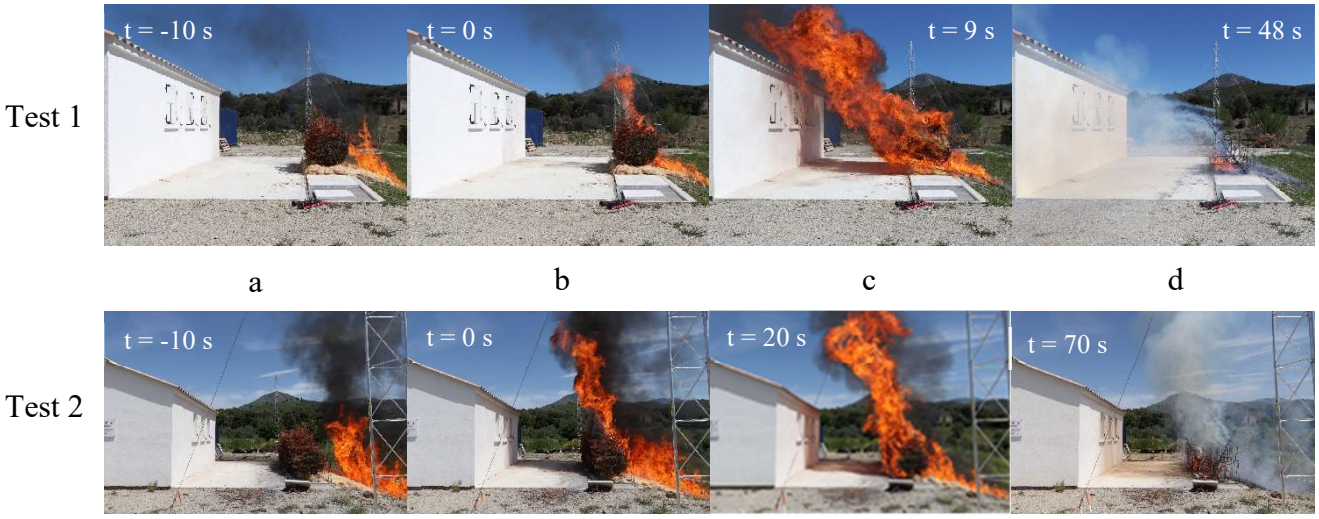

Figure 6: Photographs of the combustion phases obtained during the two tests with camera 1.a a) Fire spread in wood wool b) Ignition of the Douglas Fir trees, c) Burning of the Douglas Fir trees and d) Extinction phase

Figure 7: Fuel remaining after test 2

Figure 8 shows the mass and the mass loss rate for the two tests. In each test, the mass loss is correctly measured by the load cell. The mass measurement is not affected by the wind blowing over the vegetation or by the heat of the fire. However, the MLR is slightly noisier for test 1, which has the lowest initial mass of Douglas fir. For this test, the measurements during the smoldering phase (after 90 s) are of little use due to the inaccuracy of the load cell. In view of these results, these two experiments validate the mass monitoring system of the platform. In

both tests, the mass loss rate increases significantly after the tree ignition and reaches a peak (PMLR). For test 1, the peak occurs 9 s after the tree ignition and reaches 0.59 kg/s. For test 2, the peak is higher, 1.21 kg/s, and occurs 44 s after the ignition of the trees. The maximum MLR divided by the initial mass of Douglas fir is therefore higher for test 1 (0.034 s^{-1}) than for test 2 (0.018 s^{-1}). This is because for test 1 all the fir trees burn simultaneously, whereas for test 2, a fire spread is observed in the trees from the centre to the sides due to the V-shaped fire front coming from the burning of the wood wool and the larger number of trees. Using a ΔH_{eff} of 12,576 kJ/kg, the maximum heat release rates calculated with Eq. 1 are 7.42 MW and 15.3 MW for tests 1 and 2, respectively.

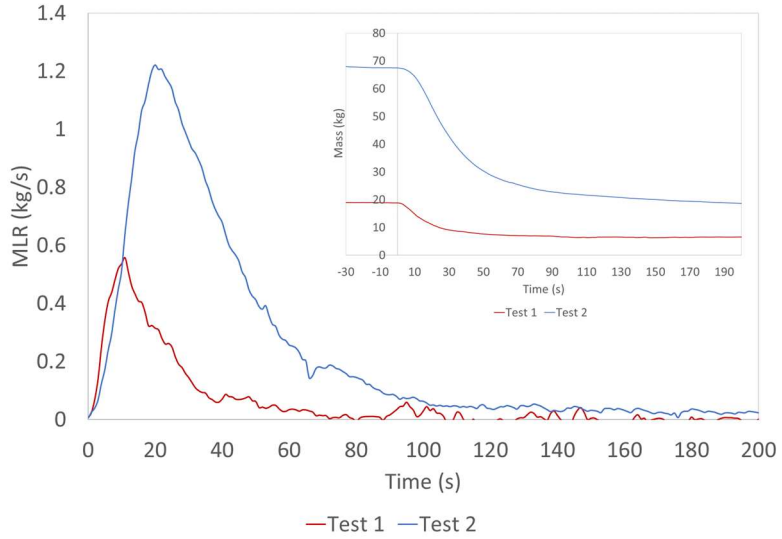

Figure 8: Mass and mass loss rate (MLR) obtained for tests 1 and 2

Figure 9 shows the profiles of the wind direction and speed measured by the anemometer on the right side (5.a in Figure 1) as well as the MLR of fir trees for test 2. Before the ignition of the wood wool (at t=-25 s for test 2), the wind has an average speed of 1.5 m/s and a direction of +9° (calculated from the data of the anemometer 5.a). As soon as the wood wool is ignited, the wind speed and direction change. Firstly, the wind direction recorded by anemometer 5.a decreases to reach a minimum value of -44°, while the wind speed increases up to 2.9 m/s. This shows that the fire tended to suck in the air from the sides of the slope. After the ignition of the trees, the wind direction becomes positive showing that the wind received by the anemometer 5.a (on the right side) comes from the flame front. This change of direction coincides with the presence of a minimum in the wind speed curve equal to 0.83 m/s.

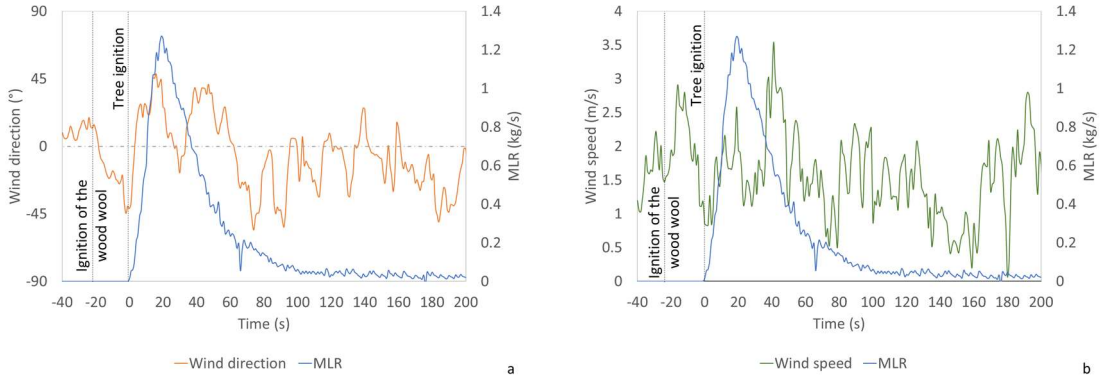

Figure 9: Evolution of MLR and a) wind direction b) wind speed – measured by the anemometer 5.a during test 2

3.2 Observation of the fire impact on the house

Figure 10 presents the mean radiant and total heat flux densities measured on the façade at a distance of 3 m from the Douglas fir trees. The averages have been calculated from the measurements by the pair of sensors placed on the facade. Figure 10.c shows the profile of the radiant heat flux measured inside the building behind the window. Table 4 presents the peak values for the heat fluxes. For all the sensors, the data is consistent. The curves of heat fluxes indeed follow the same trends as the MLR and the peaks appear at the same time. The measurements of the heat flux are within the measurement ranges. For test 1, the radiant and total heat fluxes on the facade reach 38.3 (±4.0) kW/m² and 44.4 (±1.1) kW/m², respectively. For test 2, the values are lower: 21.2 (±2.0) kW/m² and 24.6 (±0.4) kW/m² for radiant and total heat flux, respectively since the flame front advances less towards the building. For both tests, the total heat flux is higher than the radiant heat flux on average by 27.0 % during the flame duration. Although the radiant heat flux reaches 21.2 kW/m² on the facade, its value inside the house is only 2.6 kW/m². Therefore, the double-glazing acts as a screen against thermal radiation.

Figure 11 displays an example of temperatures recorded on the aluminium shutter and outside and inside glazing panels as well as the MLR for both tests. Table 4 gives the maximum temperatures of shutters and glazing panels measured for the two experiments. For both tests, the sensors did not come off and were not damaged. Given these results, the monitoring system of the fire impact on the house can be validated. In the case of test 1 with the aluminium shutters, the temperature curves obtained on the shutters are delayed in relation to that of the MLR. The rise in temperature begins a few seconds after the ignition of the fir tree and the maximum (83.9°C) is also delayed in relation to that of the MLR. This comes from the thermal properties of the shutters. With regard to the temperature of the glazing protected by the shutters, a very slight increase in the surface temperature is observed (lower than 8°C). The shutters therefore make it possible to protect the glazing against the thermal aggression of the fire. Without shutter, the temperature increase begins as soon as the flame front arrives. A maximum of 175.5°C is measured on the glazing on the exposed side. On the other hand, the temperature rise of the glazing on the interior side does not exceed 6°C during the test. For both tests carried out, we have not observed any damage to the joinery.

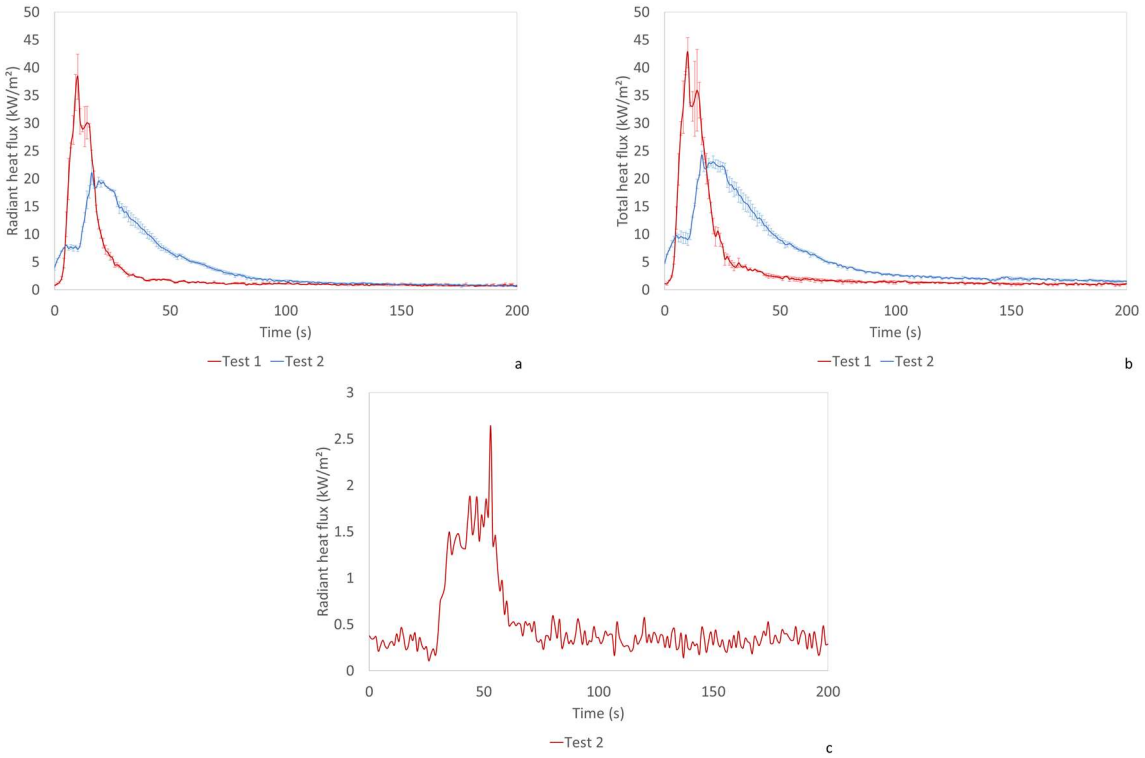

Figure 10: a) Mean radiant heat flux measured on the facade b) Mean total heat flux measured on the facade c) Radiant heat flux measured behind the window during test 2.

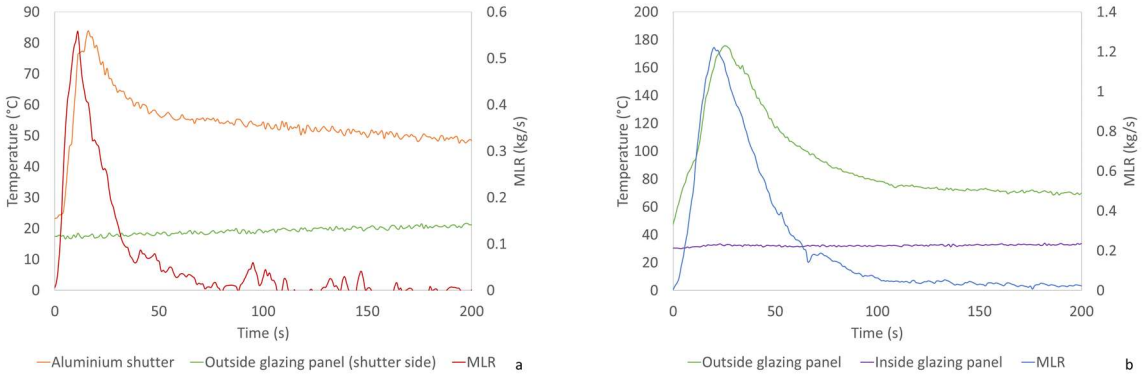

Figure 11: Mass loss rate and temperatures recorded a) on the aluminium shutter and on the outside glazing panel (side of the shutter) during test 1 b) on the outside and inside glazing panel during test 2

Table 4: Measurements recorded on the construction

Test number	Mean peak of radiant heat flux on façade (kW/m²)	Mean peak of total heat flux on facade (kW/m²)	Peak of radiant heat flux in the house (kW/m²)	Maximum temperature on shutter (°C)	Maximum temperature on outside glazing panel (°C)	Maximum temperature on inside glazing panel (°C)
1	38.3 (±4.0)	44.4 (±1.1)	-	83.9	23.6	-
2	21.2 (±2.0)	24.6 (±0.4)	2.6	-	175.5	35.5

3.3 Observation of the smoke production

Table 5 displays the emission factors (EF) of the main gases and aerosols emitted during test 2 with the smoke analysers placed outside the construction (Table 1), namely CO_2, CO, CH_4, NO_2, NH_3 and aerosols (PM). These values have been calculated based on the elementary analysis of the Douglas fir trees since the smoke has been mainly released after the tree ignition. These data are in agreement with the literature [59–64]. EF_{CO_2} and EF_{CO} are equal to 1580 and 120 g.kg^{-1} , respectively which is consistent with the studies of Andreae and Merlet [59], McMeeking et al. [64] and Soares Neto et al. [63]. The emission factor for aerosols EF_{PM} is 11 g.kg^{-1}. This is in agreement with the literature, which reports values ranging from 7.2 ± 2.3 g.kg^{-1} [59] to 11.6 ± 6.9 g.kg^{-1} [60,64] for laboratory experiments. Garcia-Hurtado et al. [65] and Alves et al. [66] provided almost identical values of 3.4 and 3.5 g.kg^{-1} for Mediterranean maquis. The emission factor for NO and NO_2 are 2.4 g.kg^{-1} and 3.2 g.kg^{-1} respectively. Overall, the average emission factor of the NO_x is higher than the values reported in the literature. For field experiments, EF_{NO_x} values between 0.3 g.kg^{-1} and 3.3 ± 1.0 g.kg^{-1} were measured [62,66,67]. The values obtained for methane ($EF_{CH_4} = 5.2$ g.kg^{-1}) and ammonia (EF_{NH_3}= 4.7 g.kg^{-1}) are higher than those observed in the literature. Akagi et al. [67] did indeed measured 1.033 ± 0.7 g.kg^{-1} and of 2.51 ± 0.7 g.kg^{-1} for NH_3 and CH_4, respectively for Chaparral. Alves et al. [66] obtained 1.3 g.kg^{-1} for ammonia during a fire in Mediterranean shrubland whereas Yokelson et al. [62] measured 1.5 ± 1.4 g.kg^{-1} for ammonia and 3.69 ± 1.4 g.kg^{-1} for methane for semiarid shrublands. Given these results, the tests validate the analyser system of the gas on the platform.

Table 5: Average EF (g.kg^{-1}) during test 2 for the gases measured by the outdoor smoke analysers.

Compounds	CO_2	CO	CH_4	CH_2O	NO	NO_2	NH_3	PM
EF (g.kg^{-1})	1580	120	5.2	3.1	2.4	3.2	4.7	11
Literature	1489-1632 [59,63,64]	50.3-104.0 [59,63,64]	2.51-3.69 [62,67]		0.3-3.3 [62,66,67]		1.03-1.50 [62,66,67]	7.2-11.6 [59,60,64]

Figure 11 presents the mass concentration of particles emitted during test 2 with the smoke analysers placed outside the construction (Table 1). The mass and particle size are given as a function of the particle sizes grouped into PM_1, $PM_{2.5}$, and PM_{10} during the advancement of the flame front. Two peaks of particle emission are observed on these curves. The first corresponds to emissions due to the burning of wood wool. The second is due to the burning of trees and is about three times higher than that recorded during the fire spread in the wood wool. The summed values for the three particle sizes are close. However, a higher peak is observed for PM_{10} and $PM_{2.5}$. According to Leonelli et al. [68], the $PM_{2.5}$ and PM_1 correspond to tar and soot, respectively. PM_{10} could be ash or dust particles suspended during the experiment. For test 1, the most abundant particle sizes are 0.3 µm and 0.4 µm. The particle analysers therefore make it possible to monitor the production of PM_1, $PM_{2.5}$ and PM_{10} during the experiments, which validates the system put in place.

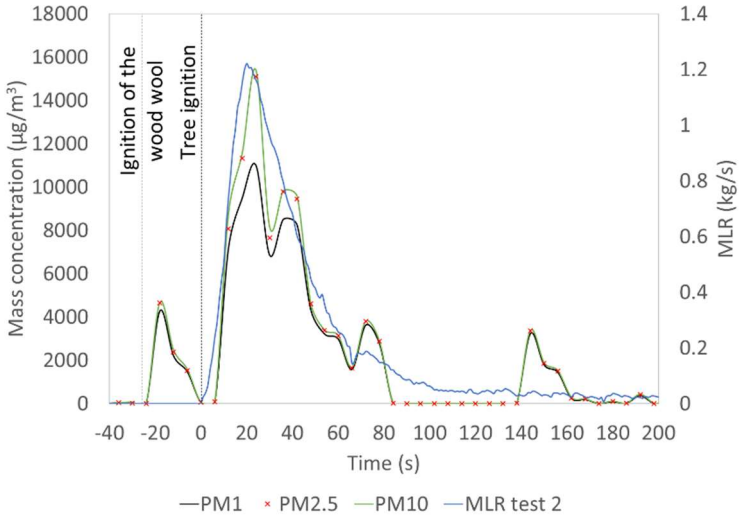

Figure 12: Mass concentration of the aerosols measured during test 2 by the outdoor smoke analyser.

3.4 Assessment of the commissioning of the EXPLORII platform

Testing of the EXPLORII platform with Douglas-fir trees during commissioning demonstrated the potential of the platform to study home vulnerability at the WUI. We were able to follow the mass loss of the fir trees and deduce the heat release rate during their burning. By means of the various cameras, we were able to follow the shape of the flames and the advance of the fire front towards the construction. The anemometers located around the platform allowed obtaining the initial wind conditions and also made it possible to see the influence of the fire on the atmospheric conditions. The radiant and total heat flux gauges as well as the thermocouples provided information on the fire impact on the building elements. The smoke analysers allowed quantification of the gases and aerosols in the smoke outside the house during the experiments.

These tests also highlighted the improvements to be made to the platform in the near future to make it more efficient. When the house is 3m from the vegetation, the flames have little inclination in the relation to the vertical. As a result, the flame front tends to mainly hit the roof. It would be interesting to add heat flux gauges to the front of the roof to obtain data at this point. It would also be interesting to add a wide-angle camera at the front of the house to give a front view. Given the recirculation of smoke observed during tests above and behind the construction, the addition of a 3D anemometer on the roof would be a valuable tool for analysing the aerology in more detail.

There are 3 main limitations to this experimental installation. Firstly, it is only possible to position the fuel 3 m from the construction if mass loss data is required. Secondly, the orientation of the platform is fixed. The wind must therefore be in the direction of the slope for optimal burning conditions. The orientation of the platform was initially chosen after analysing the wind regime at the site in order to reduce periods when the wind was unfavourable. However, some days it is not possible to carry out experiments because of the weather conditions. Finally, we opted for a sloping propagation zone in order to have a flame front with a dynamic close to that of a real fire. This reduces the number of vegetation configurations that can be tested. In order to eliminate this limitation, we are in the process of designing a motorized platform so that we can carry out both flat and sloping tests.

4 Conclusions

The EXPLORII platform was built to allow the study of the vulnerability of buildings when facing of a fire at the WUI, i.e., vegetation fires or fires from a secondary structure. The various sensors allow monitoring the aerology on the platform by means of a series of anemometers (2D and 3D), the fire dynamics using cameras and a load cell, the impact of fire on buildings by the use of heat flux gauges and thermocouples and the production and circulation of smoke.

The EXPLORII platform was successfully commissioned, providing reliable data on wind characteristics, fuel mass loss, flux received by the structure and temperature rise of its elements. In results of the experiments, the addition of new sensors (heat flux gauges, camera, anemometer) has been proposed to improve the performance of the platform. The tests performed for the commissioning of the platform have provided data on the impact of a fire on a building and on the release of smoke. These fire tests have highlighted the protective effect of the shutters, and also the role of the double glazing as a thermal screen. Continuing to conduct experiments on the EXPLORII platform will make it possible to collect field-scale data on the vegetation burning, the potential damage of vegetation fire on constructions and health impacts of fire at the WUI. This data is crucial in fire prevention. The large-scale experiments carried out on the EXPLORII platform will also allow researchers and industry to develop effective mitigation measures, such as fire-resistant materials or smart landscaping. The EXPLORII platform will also make it possible to study the complex interactions between different factors that significantly influence the spread, intensity and impact of fires, such as wind or fuels (species, moisture, layout). Having data acquired under realistic conditions is essential for the development of robust fire safety regulations and guidelines. The EXPLORII platform has been designed for this purpose.

Declaration of funding

This research was supported by the projects "MED-STAR" (Strategie e misure per la mitigazione del rischio di incendio nell'area Mediterranea) and "INTERMED" (Interventions pour gérer et réduire le risque d'incendie à l'interface habitat-espace naturel) financed by the fund PC IFM 2014-2020 (http://interreg-maritime.eu/fr/web/med-star).

References

[1] A. Ganteaume, A. Camia, M. Jappiot, J. San-Miguel-Ayanz, M. Long-Fournel, C. Lampin, A Review of the Main Driving Factors of Forest Fire Ignition Over Europe, Environmental Management. 51 (2013) 651–662. https://doi.org/10.1007/s00267-012-9961-z.

[2] M.A. Moritz, M.E. Morais, L.A. Summerell, J.M. Carlson, J. Doyle, Wildfires, complexity, and highly optimized tolerance, Proc. Natl. Acad. Sci. U.S.A. 102 (2005) 17912–17917. https://doi.org/10.1073/pnas.0508985102.

[3] W.M. Jolly, M.A. Cochrane, P.H. Freeborn, Z.A. Holden, T.J. Brown, G.J. Williamson, D.M.J.S. Bowman, Climate-induced variations in global wildfire danger from 1979 to 2013, Nat Commun. 6 (2015) 7537. https://doi.org/10.1038/ncomms8537.

[4] P. Vacca, D. Caballero, E. Pastor, E. Planas, WUI fire risk mitigation in Europe: A performance-based design approach at home-owner level, Journal of Safety Science and Resilience. 1 (2020) 97–105. https://doi.org/10.1016/j.jnlssr.2020.08.001.

[5] K. Haynes, K. Short, G. Xanthopoulos, D. Viegas, L.M. Ribeiro, R. Blanchi, Wildfires and WUI Fire Fatalities, in: S.L. Manzello (Ed.), Encyclopedia of Wildfires and

Wildland-Urban Interface (WUI) Fires, Springer International Publishing, Cham, 2020: pp. 1–16. https://doi.org/10.1007/978-3-319-51727-8_92-1.
[6] R. Blanchi, J.E. Leonard, R.H. Leicester, Lessons learnt from post-bushfire surveys at the urban interface in Australia, Forest Ecology and Management. 234 (2006) S139. https://doi.org/10.1016/j.foreco.2006.08.184.
[7] A. Maranghides, D. McNamara, R. Vihnanek, J. Restaino, C. Leland, A Case Study of a Community Affected by the Waldo Fire Event Timeline and Defensive Actions, NIST, 2015.
[8] A. Maranghides, W. Mell, A Case Study of a Community Affected by the Witch and Guejito Wildland Fires, Fire Technology. 47 (2011) 379–420. https://doi.org/10.1007/s10694-010-0164-y.
[9] J. Laranjeira, H. Cruz, Building vulnerabilities to fires at the wildland urban interface, in: Advances in Forest Fire Research, Imprensa da Universidade de Coimbra, 2014: pp. 673–684. https://doi.org/10.14195/978-989-26-0884-6_76.
[10] B. Gaudet, A. Simeoni, S. Gwynne, E. Kuligowski, N. Benichou, A review of post-incident studies for wildland-urban interface fires, Journal of Safety Science and Resilience. 1 (2020) 59–65. https://doi.org/10.1016/j.jnlssr.2020.06.010.
[11] A. Westhaver, Why Some Homes Survived: Learning from the Fort Mcmurray Wildland/urban Interface Fire Disaster, ICLR Research Paper Series - Number 56. (2017). https://www.deslibris.ca/ID/10091218 (accessed July 24, 2022).
[12] S. Manzello, Special Issue on Wildland–Urban Interface (WUI) Fires, Fire Technology. 50 (2014). https://doi.org/10.1007/s10694-012-0319-0.
[13] A. Ganteaume, Role of the ornamental vegetation in the propagation of the Rognac fire (SE France, 2016), in: Missoula, 2018.
[14] N. Flores Quiroz, L. Gibson, W.S. Conradie, P. Ryan, R. Heydenrych, A. Moran, A. van Straten, R. Walls, Analysis of the 2017 Knysna fires disaster with emphasis on fire spread, home losses and the influence of vegetation and weather conditions: A South African case study, International Journal of Disaster Risk Reduction. 88 (2023) 103618. https://doi.org/10.1016/j.ijdrr.2023.103618.
[15] T. Barboni, M. Cannac, V. Pasqualini, A. Simeoni, E. Leoni, N. Chiaramonti, Volatile and semi-volatile organic compounds in smoke exposure of firefighters during prescribed burning in the Mediterranean region, Int. J. Wildland Fire. 19 (2010) 606. https://doi.org/10.1071/WF08121.
[16] T. Barboni, L. Leonelli, P.-A. Santoni, V. Tihay-Felicelli, Influence of particle size on the heat release rate and smoke opacity during the burning of dead Cistus leaves and twigs, Journal of Fire Sciences. 35 (2017) 259–283. https://doi.org/10.1177/0734904117709964.
[17] P.-A. Santoni, E. Romagnoli, N. Chiaramonti, T. Barboni, Scale effects on the heat release rate, smoke production rate, and species yields for a vegetation bed, Journal of Fire Sciences. 33 (2015) 290–319. https://doi.org/10.1177/0734904115591176.
[18] T. Barboni, L. Leonelli, P.-A. Santoni, V. Tihay-Felicelli, Aerosols and carbonaceous and nitrogenous compounds emitted during the combustion of dead shrubs according to twigs' diameter and combustion phases, Fire Safety Journal. 113 (2020) 102988. https://doi.org/10.1016/j.firesaf.2020.102988.
[19] National Fire Protection Association, Preparing homes for wildfire, (2022). https://www.nfpa.org/Public-Education/Fire-causes-and-risks/Wildfire/Preparing-homes-for-wildfire.
[20] Regione Toscana, Piano AIB 2019-2021 (art. 74 L.R. 39/00), Giunta Regione Toscana, 2019.
[21] FireSmart, About FireSmart, (2022). https://firesmartcanada.ca/about-firesmart/.

[22] Prefet de la Haute Corse, Arrêté DDT2B/SEBF/FORET/N° 2B-2022-04-05-00006 En date du 05 avril 2022 relatif au débroussaillement légal, 2022.
[23] Republica portuguesa, Campanha de limpeza do mato, (2018). https://www.portugal.gov.pt/pt/gc21/comunicacao/noticia?i=campanha-de-limpeza-do-mato.
[24] Standards Australia Committee, Australian standard–construction of buildings in bushfire-prone areas AS 3959-2009, (2009).
[25] ASTM International, Standard Test Method for Evaluating the Fire-Test-Response of Deck Structures to Burning Brands, (2012).
[26] ASTM International, Test Method for Evaluating the Under-Deck Fire Test Response of Deck Materials, (2013).
[27] Japanese Standards Association (JSA), JIS A 1310 - Test method for fire propagation over building façades, (2019).
[28] ISO/TC 92 Fire safety, ISO/TR 24188:2022 - Large outdoor fires and the built environment — Global overview of different approaches to standardization, (2022).
[29] S.E. Caton, R.S.P. Hakes, D.J. Gorham, A. Zhou, M.J. Gollner, Review of Pathways for Building Fire Spread in the Wildland Urban Interface Part I: Exposure Conditions, Fire Technol. 53 (2017) 429–473. https://doi.org/10.1007/s10694-016-0589-z.
[30] B.W. Butler, J. Cohen, D.J. Latham, R.D. Schuette, P. Sopko, K.S. Shannon, D. Jimenez, L.S. Bradshaw, Measurements of radiant emissive power and temperatures in crown fires, Canadian Journal of Forest Research. 34 (2004) 1577–1587.
[31] J.D. Cohen, Relating flame radiation to home ignition using modeling and experimental crown fires, Canadian Journal of Forest Research. 34 (2004) 1616–1626.
[32] B. Porterie, J.-L. Consalvi, J.-C. Loraud, F. Giroud, C. Picard, Dynamics of wildland fires and their impact on structures, Combustion and Flame. 149 (2007) 314–328. https://doi.org/10.1016/j.combustflame.2006.12.017.
[33] S. Suzuki, S.L. Manzello, Experimental Study on Vulnerabilities of Japanese-Style Tile Roof Assemblies to Firebrand Exposures, Fire Technology. 56 (2020) 2315–2330. https://doi.org/10.1007/s10694-020-00982-2.
[34] S. Suzuki, S.L. Manzello, Experiments to provide the scientific-basis for laboratory standard test methods for firebrand exposure, Fire Safety Journal. 91 (2017) 784–790. https://doi.org/10.1016/j.firesaf.2017.03.055.
[35] S.L. Manzello, S.-H. Park, S. Suzuki, J.R. Shields, Y. Hayashi, Experimental investigation of structure vulnerabilities to firebrand showers, Fire Safety Journal. 46 (2011) 568–578. https://doi.org/10.1016/j.firesaf.2011.09.003.
[36] S.L. Manzello, S. Suzuki, Experimental investigation of wood decking assemblies exposed to firebrand showers, Fire Safety Journal. 92 (2017) 122–131. https://doi.org/10.1016/j.firesaf.2017.05.019.
[37] T.Z. Fabian, Fire Performance Properties of Solid Wood and Lignocellulose-Plastic Composite Deck Boards, Fire Technol. 50 (2014) 125–141. https://doi.org/10.1007/s10694-012-0307-4.
[38] L.E. Hasburgh, D.S. Stone, S.L. Zelinka, Laboratory Investigation of Fire Transfer from Exterior Wood Decks to Buildings in the Wildland–Urban Interface, Fire Technol. 53 (2017) 517–534. https://doi.org/10.1007/s10694-016-0588-0.
[39] V. Tihay-Felicelli, K. Meerpoel-Pietri, P.A. Santoni, F. Morandini, A. Pieri, T. Barboni, Flammability study of decking sections found at the Wildland–Urban interface at different scales, Fire Safety Journal. 139 (2023) 103838. https://doi.org/10.1016/j.firesaf.2023.103838.
[40] F.W. Mowrer, Window Breakage Induced by Exterior Fires, National Institute of Standards and Technology, 1998.

[41] J.D. Cohen, Structure ignition assessment model (SIAM)1, In: Weise, David R.; Martin, Robert E., Technical Coordinators. The Biswell Symposium: Fire Issues and Solutions in Urban Interface and Wildland Ecosystems; February 15-17, 1994; Walnut Creek, California. Gen. Tech. Rep. PSW-GTR-158. Albany, CA: Pacific Southwest Research Station, Forest Service, U.S. Department of Agriculture; p. 85-92. 158 (1995). https://www.fs.usda.gov/treesearch/pubs/27418 (accessed September 19, 2021).
[42] B.R. Cuzzillo, P.J. Pagni, Thermal Breakage of Double-Pane Glazing By Fire, Journal of Fire Protection Engineering. 9 (1998) 1–11. https://doi.org/10.1177/104239159800900101.
[43] Y. Wang, Q. Wang, Y. Su, J. Sun, L. He, K.M. Liew, Fracture behavior of framing coated glass curtain walls under fire conditions, Fire Safety Journal. 75 (2015) 45–58. https://doi.org/10.1016/j.firesaf.2015.05.002.
[44] K. Harada, A. Enomoto, K. Uede, T. Wakamatsu, An Experimental Study On Glass Cracking And Fallout By Radiant Heat Exposure, Fire Saf. Sci. 6 (2000) 1063–1074. https://doi.org/10.3801/IAFSS.FSS.6-1063.
[45] J.W. van de Lindt, S.E. Pryor, S. Pei, Shake table testing of a full-scale seven-story steel–wood apartment building, Engineering Structures. 33 (2011) 757–766. https://doi.org/10.1016/j.engstruct.2010.11.031.
[46] Joint Research centre European Commission, ELSA European Laboratory for Structural Assessment, (2022). http://www.samco.org/download/jrc.pdf.
[47] Design Safe, About NHERI the Natural Hazards Engineering Research Infrastructure, (n.d.). https://www.designsafe-ci.org/about/.
[48] NIST, National Fire Research Laboratory, (n.d.). https://www.nist.gov/el/fire-research-division-73300/national-fire-research-laboratory-73306.
[49] Building Research Institute, Department of Fire Engineering, (n.d.). https://www.kenken.go.jp/english/research/fir/index.html.
[50] National Research Institute of dire and Disaster, Research facilities, (n.d.). https://nrifd.fdma.go.jp/english/about/research_facilities/index.html (accessed June 5, 2023).
[51] CSIRO, The National Bushfire Behaviour Research Laboratory at CSIRO Black Mountain, Canberra, (n.d.). https://www.csiro.au/en/work-with-us/use-our-labs-facilities/bushfire-laboratory (accessed June 6, 2023).
[52] M. Bundy, A. Hamins, J. Gross, W. Grosshandler, L. Choe, Structural Fire Experimental Capabilities at the NIST National Fire Research Laboratory, Fire Technol. 52 (2016) 959–966. https://doi.org/10.1007/s10694-015-0544-4.
[53] Building Research Institute, Fire Wind Tunnel, (n.d.). https://www.kenken.go.jp/english/pdf/03.pdf (accessed June 6, 2023).
[54] S.L. Manzello, J.R. Shields, T.G. Cleary, A. Maranghides, W.E. Mell, J.C. Yang, Y. Hayashi, D. Nii, T. Kurita, On the development and characterization of a firebrand generator, Fire Safety Journal. 43 (2008) 258–268. https://doi.org/10.1016/j.firesaf.2007.10.001.
[55] Building Research Institute, Full Scale Fire Test Laboratory, (n.d.). https://www.kenken.go.jp/english/pdf/02.pdf (accessed June 6, 2023).
[56] A.L. Sullivan, I.K. Knight, R.J. Hurley, C. Webber, A contractionless, low-turbulence wind tunnel for the study of free-burning fires, Experimental Thermal and Fluid Science. 44 (2013) 264–274. https://doi.org/10.1016/j.expthermflusci.2012.06.018.
[57] Suncorp, One house to save many, (n.d.). https://onehouse.suncorp.com.au/.
[58] V. Tihay-Felicelli, P.A. Santoni, G. Gerandi, T. Barboni, Smoke emissions due to burning of green waste in the Mediterranean area: Influence of fuel moisture content and

fuel mass, Atmospheric Environment. 159 (2017) 92–106. https://doi.org/10.1016/j.atmosenv.2017.04.002.
[59] M.O. Andreae, P. Merlet, Emission of trace gases and aerosols from biomass burning, Global Biogeochemical Cycles. 15 (2001) 955–966. https://doi.org/10.1029/2000GB001382.
[60] J. Aurell, B.K. Gullett, D. Tabor, Emissions from southeastern U.S. Grasslands and pine savannas: Comparison of aerial and ground field measurements with laboratory burns, Atmospheric Environment. 111 (2015) 170–178. https://doi.org/10.1016/j.atmosenv.2015.03.001.
[61] E. Romagnoli, T. Barboni, P.-A. Santoni, N. Chiaramonti, Quantification of volatile organic compounds in smoke from prescribed burning and comparison with occupational exposure limits, Nat. Hazards Earth Syst. Sci. 14 (2014) 1049–1057. https://doi.org/10.5194/nhess-14-1049-2014.
[62] R.J. Yokelson, I.R. Burling, J.B. Gilman, C. Warneke, C.E. Stockwell, J. de Gouw, S.K. Akagi, S.P. Urbanski, P. Veres, J.M. Roberts, W.C. Kuster, J. Reardon, D.W.T. Griffith, T.J. Johnson, S. Hosseini, J.W. Miller, D.R. Cocker III, H. Jung, D.R. Weise, Coupling field and laboratory measurements to estimate the emission factors of identified and unidentified trace gases for prescribed fires, Atmos. Chem. Phys. 13 (2013) 89–116. https://doi.org/10.5194/acp-13-89-2013.
[63] T.G. Soares Neto, J.A. Carvalho, E.V. Cortez, R.G. Azevedo, R.A. Oliveira, W.R.R. Fidalgo, J.C. Santos, Laboratory evaluation of Amazon forest biomass burning emissions, Atmospheric Environment. 45 (2011) 7455–7461. https://doi.org/10.1016/j.atmosenv.2011.05.003.
[64] G.R. McMeeking, S.M. Kreidenweis, S. Baker, C.M. Carrico, J.C. Chow, J.L. Collett, W.M. Hao, A.S. Holden, T.W. Kirchstetter, W.C. Malm, H. Moosmüller, A.P. Sullivan, C.E. Wold, Emissions of trace gases and aerosols during the open combustion of biomass in the laboratory, J. Geophys. Res. 114 (2009) D19210. https://doi.org/10.1029/2009JD011836.
[65] E. Garcia-Hurtado, J. Pey, M.J. Baeza, A. Carrara, J. Llovet, X. Querol, A. Alastuey, V.R. Vallejo, Carbon emissions in Mediterranean shrubland wildfires: An experimental approach, Atmospheric Environment. 69 (2013) 86–93. https://doi.org/10.1016/j.atmosenv.2012.11.063.
[66] C.A. Alves, C. Gonçalves, C.A. Pio, F. Mirante, A. Caseiro, L. Tarelho, M.C. Freitas, D.X. Viegas, Smoke emissions from biomass burning in a Mediterranean shrubland, Atmospheric Environment. 44 (2010) 3024–3033. https://doi.org/10.1016/j.atmosenv.2010.05.010.
[67] S.K. Akagi, R.J. Yokelson, C. Wiedinmyer, M.J. Alvarado, J.S. Reid, T. Karl, J.D. Crounse, P.O. Wennberg, Emission factors for open and domestic biomass burning for use in atmospheric models, Atmos. Chem. Phys. 11 (2011) 4039–4072. https://doi.org/10.5194/acp-11-4039-2011.
[68] L. Leonelli, T. Barboni, P.A. Santoni, Y. Quilichini, A. Coppalle, Characterization of aerosols emissions from the combustion of dead shrub twigs and leaves using a cone calorimeter, Fire Safety Journal. 91 (2017) 800–810. https://doi.org/10.1016/j.firesaf.2017.03.048.